Theory for optimal design of waveguiding light concentrators in photovoltaic microcell arrays

Andrey V. Semichaevsky,[1,*] Harley T. Johnson,[1,2] Jongseung Yoon,[3] Ralph G. Nuzzo,[2] Lanfang Li,[2] and John Rogers[1,2]

[1]Department of Mechanical Science and Engineering, University of Illinois at Urbana-Champaign, 1206 West Green Street, Urbana, Illinois 61801, USA

[2]Department of Materials Science and Engineering, University of Illinois at Urbana-Champaign, 1304 West Green Street, Urbana, Illinois 61801, USA

[3]Mork Family Department of Chemical Engineering and Materials Science, University of Southern California, VHE 518, 3651 Watt Way, Los Angeles, California 90089, USA

*Corresponding author: avsemych@uiuc.edu

Received 28 March 2011; accepted 12 April 2011;
posted 15 April 2011 (Doc. ID 144877); published 9 June 2011

Efficiency of ultrathin flexible solar photovoltaic silicon microcell arrays can be significantly improved using nonimaging solar concentrators. A fluorophore is introduced to match the solar spectrum and the low-reflectivity wavelength range of Si, reduce the escape losses, and allow the nontracking operation. In this paper we optimize our solar concentrators using a luminescent/nonluminescent photon transport model. Key modeling results are compared quantitatively to experiments and are in good agreement with the latter. Our solar concentrator performance is not limited by the dye self-absorption. Bending deformations of the flexible solar collectors do not result in their indirect gain degradation compared to flat solar concentrators with the same projected area.

OCIS codes: 350.6050, 220.1770, 220.4298.

1. Introduction

Ultrathin flexible photovoltaic (PV) microcell arrays that use less silicon per area than conventional PV cell panels have recently been demonstrated [1]. Such structures, by definition, have large spaces between PV cells, so concentrating optics must be added to better utilize the incident solar photon flux. An application of a microlens array for this purpose has been discussed, implemented, and tested experimentally [1]. However, a microlens-based solar concentrator requires precise optical alignment and is highly sensitive to the light incidence direction.

As an alternative to the microlens concentrator, we consider a microcell array design featuring a planar dielectric waveguide with a total internal reflection (TIR) condition along the top side and a specular or a diffuse reflector on the other side to illuminate all surfaces of the microcells, thereby increasing the photon flux absorbed in the PV cells. Luminescent [2–5] and nonluminescent [6,7] waveguiding solar concentrators have widely been used in PV technology. However, unlike the previous waveguiding solar concentrator designs in which a solar cell is side-mounted, in our structure, solar microcells are embedded in a very weakly scattering polymer layer along the top surface and are directly exposed to sunlight on one side. The solar concentrator for the microcell array collects the photons incident on the gaps between the PV cells and redirects them into the semiconductor material where they are absorbed and contribute to the photocurrent. Therefore, the flexible structure of the microcell array itself serves as a highly multimodal optical waveguide, and, in case of a guiding layer doped with a luminescent dye, also converts the wavelengths of a portion of

0003-6935/11/172799-10$15.00/0

the photon flux to the low-reflectivity range of the semiconductor. Because of the use of a backside reflector (BSR), this design can work either with or without luminescence, although, as our simulations and experiments show, its performance is better in the presence of a luminescent dye.

In this paper, we analyze the performance of waveguiding solar concentrators for thin Si microcell arrays using a simplified geometrical optics approach and the coupled power theory [8–10], and we provide recommendations regarding geometrical parameters that maximize the solar light absorption in Si microcells. The indirect gain of the concentrator depends on the widths of the microcells relative to the period of the microcell array (microcell fill factor) and the substrate layer thickness relative to the microcell width (a/W). The substrate layer material is chosen with a refractive index that is close to the index of the embedding polymer layer.

The thickness of the Si microcells is yet another parameter affecting the light absorption. The geometry and the key dimensions of a PV microcell array are shown schematically in Fig. 1. We also explore the changes in the device performance when the microcell array is bent in the x-z plane.

In the case of a luminescent concentrator, there are also several additional parameters: the thickness of the luminescent layer and the absorption and emission spectra of the luminophore that are functions of its concentration. As we show later in this paper, the thicknesses of Si microcells should be sufficiently large to trap the incident photons of most energies above the semiconductor bandgap. Microcells made of a direct bandgap semiconductor, such as GaAs, with a higher absorption coefficient, can be significantly thinner than those made of silicon. The goal of this study is to identify optimal geometries of solar concentrators for microcell arrays so that the indirect gain, defined as a ratio of absorbed photon flux due to indirect illumination over the absorbed photon flux under direct illumination and without any reflector, is maximized. Spectral properties of various luminescent dyes are included in our intensity transport model explicitly, along with dye self-absorption effects. Effective photon extinction length inside the guiding layer, apart from its geometry and photon absorption in the Si microcells, depends on the properties of the waveguiding layer material. These properties include the refractive index of the polymer matrix and the type of dye and its concentration, and they determine the absorption, dye emission, self-absorption, and thermalization losses associated with the photon energy downshift. For this reason, the geometry optimization presented here for a luminescent concentrator is mostly illustrative, but for a nonluminescent concentrator, the optimization results can be readily generalized.

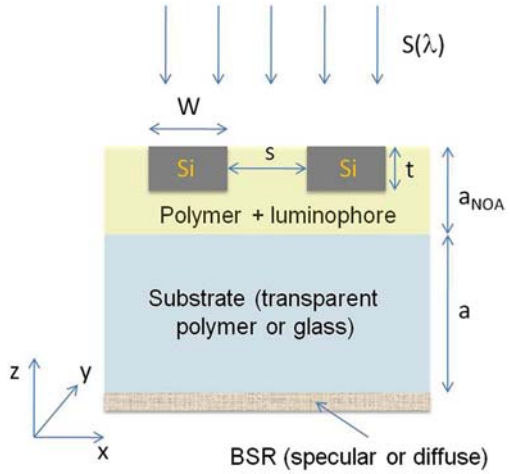

Fig. 1. (Color online) Cross section of the solar concentrator for ultrathin Si microcells.

Our simulation results suggest that the photon flux absorbed by microcells increases up to a saturation level as the area fill factor of Si decreases, for both the nonluminescent and luminescent solar concentrators. The same parameter as a function of the ratio of the substrate layer thickness (assuming that the substrate material is glass) to the microcell width (a/W) has an optimum. Another significant parameter affecting the performance of the PV ultrathin microcell array is the microcell thickness (t). The microcell thickness influences both the absorption of the incident light in silicon and the surface area of the device indirectly exposed to sunlight.

The luminescent dye chosen for our luminescent concentrator, dicyanomethylene, has properties that are close to optimal when silicon is used as the semiconductor in PV microcells. For the typical dye concentrations, the light extinction length in the collector due to self-absorption is several orders of magnitude longer than the spacing between PV microcells; therefore, self-absorption only has minor effects on the concentrator performance.

According to our model, antireflection coatings (ARC) applied on the top and the side surfaces of the Si microcells can further increase the absorbed photon flux in our microcells by about 46%, in addition to the gain due to photons absorbed from indirect illumination.

Solar concentrators with microcell arrays printed on the top of the waveguiding layer are found to have substantially higher collection efficiencies compared to those in which solar panels are side mounted. Our designs are also relatively insensitive to bending deformations and do not degrade the solar concentrator performance.

2. Theory

There are numerous studies on the design and analysis of performance of luminescent [2,5] and nonluminescent solar concentrators [6,7] for PV cells in the literature. However, our thin microcell design utilizing micron-scale semiconductor devices is different from those considered previously since the PV microcell arrays are embedded in a polymer layer along the top surface of the structure, are directly exposed to sunlight on one side, and can also admit photons

through other surfaces with the help of the waveguiding polymer layer. The Si microcells are fabricated in such a way that their Ohmic n^+ and p^+ contacts are on the top surfaces, and interconnects are printed on the top of the structure.

Various elements of the PV microcell array are shown in Fig. 1. The solar photon flux incident on the top surfaces of Si microcells is partially absorbed by them, while the portion of the incident photon flux incident on the gaps between the cells propagates through the polymer and the substrate layers and strikes the reflector. The polymer layer, for instance, dicyanomethylene (DCM) 61 [11], can be doped with luminescent dye molecules, in which case a portion of incoming light is absorbed and reemitted isotropically in a longer wavelength range. The BSR and the luminescent material both randomize the angular spectrum of the incident sunlight. This is important for the energy harvesting from a larger area due to waveguiding.

When the polymer layer is doped with a luminescent dye, the waveguiding is also accompanied by the spectral conversion. The dye-doped polymer layer in our structure, thus, serves three purposes: randomization of light propagation directions, isotropic emission resulting in lower non-TIR waveguiding losses, as we will show later, and the spectral matching between the emitted light spectrum and the low-reflectivity wavelength range of the semiconductor material. The Norland optical adhesive (NOA) 61 polymer matrix has very low absorption above 400 nm and is, therefore, suitable for the waveguiding layer fabrication.

The scattering losses due to non-TIR angular spectral components in a dye-doped dielectric waveguide are expected to be lower than those in a nonluminescent waveguide because of isotropic emission by luminophore molecules. For the first generation of photons scattered off by a Lambertian diffuse reflector and reflected by the polymer-air interface, the fraction of light intensity carried by the angular modes undergoing TIR is substantially higher for isotropically emitted light than for a nonluminescent transparent polymer layer. To analyze this quantitatively, we first consider a simple case similar to that shown in Fig. 1 but without Si microcells on the top, and with the BSR in direct contact with the polymer layer (either transparent or luminescent). In this case, the fraction of input photon flux propagating by TIR without luminescence $f_{\mathrm{TIR},nl}$, and with the luminescence, considering only the first generation of emitted photons and a perfect Lambertian diffuse reflector $f_{\mathrm{TIR},l}$, are given by

$$f_{\mathrm{TIR},nl} = \frac{1}{\pi}\int_{-\pi}^{\pi}\int_{\theta_{\mathrm{TIR}}}^{\pi/2}\cos\theta\sin\theta\mathrm{d}\theta\mathrm{d}\phi, \tag{1a}$$

$$f_{\mathrm{TIR},l} = \int_{-\pi}^{\pi}\int_{\theta_{\mathrm{TIR}}}^{\pi/2}\frac{1}{4\pi}\sin\theta\mathrm{d}\theta\mathrm{d}\phi + \frac{1}{2\pi}\int_{-\pi}^{\pi}\int_{\theta_{\mathrm{TIR}}}^{\pi/2}\cos\theta\sin\theta\mathrm{d}\theta\mathrm{d}\phi. \tag{1b}$$

For instance, if $n_{\mathrm{NOA}} = 1.6$, $\theta_{\mathrm{TIR}} = 0.675$, then $f_{\mathrm{TIR},nl} = 0.325$, and $f_{\mathrm{TIR},l} = 0.553$. Thus, in the absence of self-absorption, isotropically emitted angular modes can propagate in the collector with lower losses per unit length than the ones that are normally incident on the diffuse reflector. In addition to lower propagation losses, the photocurrent from a microcell array embedded in a luminescent medium is further enhanced because the spectral content of the light is converted to a wavelength range where the polymer-Si interface has lower reflectivity. Energy losses associated with the downshift and the photon escape from the collector can be offset by the gains in the absorbed photon flux described above. There are two primary factors that affect how the absorbed photon flux depends on the spacing between the cells, as well as on the microcell width, W, and on the thickness of substrate, a, namely, the waveguiding losses (due to the modes escaping from the waveguiding polymer layer into the air or laterally outside of the microcell array) and the self-absorption losses in the luminescent medium.

We treat both of these mechanisms explicitly in our model as described below. First we assume that solar light with spectral irradiance $S(\lambda)$, given by the AM1.5G spectrum [12], is incident normally on an array of Si microcells of area $A = A_{\mathrm{top}} + A_{\mathrm{NOA}} = L(W + s)$, embedded in a transparent polymer layer, as illustrated in Fig. 1, where L is the length of the structure along the y axis. Then the input solar power and the cell efficiency are defined as

$$P_{\mathrm{in}} = A\int S(\lambda)\mathrm{d}\lambda, \tag{2a}$$

$$\eta = \frac{P_{\mathrm{out}}}{P_{\mathrm{in}}}, \tag{2b}$$

where P_{out} is the output electric power of the cell.

Taking into account the spectral internal quantum efficiency of the silicon p-n junction $\eta_q(\lambda)$, P_{out} can then be obtained from

$$P_{\mathrm{out}} = \frac{qV_{\mathrm{oc}}\mathrm{FF}}{hc}\int_0^{\lambda_{g,\mathrm{Si}}}\eta_q(\lambda)\left(\int_{A_{\mathrm{exp}}}\Phi_0(r,\lambda)\mathrm{d}A + \int_{A_{\mathrm{ind}}}\Phi_{\mathrm{ind}}(r,\lambda)\mathrm{d}A\right)\lambda\mathrm{d}\lambda, \tag{3}$$

where V_{oc} is the open circuit voltage of the PV cell and FF its voltage fill factor determined from the cell I-V curve. A_{exp} is the microcell surface directly exposed to sunlight, A_{ind} is the microcell surface, indirectly exposed to sunlight, and dA is the surface differential. In our devices [1], about 90% of the top surface area is exposed to direct illumination for the interconnected microcell arrays used in the bending experiments. In all other experiments, there are no interconnects blocking the sunlight, and electrical characteristics of the cells are measured via pin probes. The photon flux spectral density Φ_0 serving as a reference, is absorbed through the top surface

when the microcell is above a black surface, while Φ_{ind} (either nonluminescent or luminescent) is absorbed via microcell surfaces other than the top surface (due to indirect illumination).

Since the internal quantum efficiency (IQE) of a PV cell requires complex carrier transport calculations that are beyond the scope of the PV cell geometry designs, we use the indirect gain in the photon flux as a figure of merit in our calculations. This indirect gain, k_Φ, is independent of the IQE and is given by

$$k_\Phi = \frac{\int_0^{\lambda_g}\left\{\int_{A_{\text{exp}}}\Phi_0(r,\lambda)\mathrm{d}A + \int_{A_{\text{ind}}}\Phi_{\text{ind}}(r,\lambda)\mathrm{d}A\right\}\mathrm{d}\lambda}{A\int\Phi_0(\lambda)\mathrm{d}\lambda}, \quad (4)$$

where $\Phi(\lambda)$ is the solar photon flux spectral density absorbed into Si through all the surfaces of the microcells, and subscript "ind" stands for "indirect." We assume that the top surfaces of the Si microcells are not coated with NOA, since such a coating would interfere with pin probe electrical characterization, and we also do not use any AR coatings on the microcells since bare Si reflectivity has a well-known wavelength dependence and is, therefore, a better standard reference configuration than an AR-coated Si surface whose reflectance spectrum depends on a particular type of an AR coating.

Besides the indirect gain of a single microcell, we also consider the gain in the microcell array (module) efficiency, with respect to a thick continuous silicon panel of the same area, given by

$$k_{\Phi,m} = hc \times \frac{\int_0^{\lambda_g}\left\{\sum_{i=1}^{N}\int_{A\text{exp}}\Phi_{0,i}(r,\lambda)\mathrm{d}A + \int_{A\text{ind}}\Phi_{\text{ind},i}(r,\lambda)\mathrm{d}A\right\}\mathrm{d}\lambda}{\int_0^{\lambda_g}\{A_{\text{exp}}S(\lambda)(1-R(\lambda))\}\lambda\mathrm{d}\lambda}, \quad (5)$$

where A_{exp} is assumed to be the whole top area of a PV cell, and $R(\lambda)$ is the reflectivity of the bare Si-air interface.

In this case, the numerator includes the sum of photon fluxes absorbed by all microcells, and the denominator is the total photon flux absorbed by a thick continuous PV panel.

The analysis of the light interaction with our solar concentrator is carried out in the geometrical optics approximation, since all dimensions of the devices are at least 20 times greater than the longest light wavelength. A physical optics picture of the diffuse reflector scattering is not included because of its high complexity. Instead, a statistical Monte Carlo technique [13], similar to the approach discussed in [9,10], is used. The number of individual rays necessary for satisfactory convergence of the Monte Carlo method depends on the concentrator geometry and material properties; it is found empirically that about 10,000 rays provide $<1\%$ accuracy for the solar concentrator structures considered in this paper. The reflections from and transmissions through surfaces other than the reflector are calculated using the average Fresnel power reflection coefficients for TE and TM polarizations (7), to account for the randomly polarized solar light.

Our approach to modeling a dielectric waveguide with rough surface reflectors is based on the coupled power theory [8], in which we consider a very large number of angular modes coupled in a statistical sense at the surface of the BSR. Thus, a single mode incident on a diffuse reflector produces a random distribution of scattered modes with uniformly distributed scattering directions, and the coupling constants between the spectral irradiances of the modes at the rough surface interface are found using the angular-dependent reflectivity of the reflector, $R(\theta',\theta)$. In case of the specular reflector, no coupling between the modes is assumed. Modes (rays) with random propagation directions are also assumed in the modeling of the luminescent dyes. For simplicity, a diffuse BSR is modeled as Lambertian, with the angular distribution of reflected intensities given as $R = R_0\cos(\theta)$, regardless of the incidence direction. A more accurate model of a diffuse reflector can also be implemented using autocovariance functions of experimental rough surface profiles [10]. A 3D geometrical optics model of a large array of microcells embedded in a luminescent medium and backed with a reflecting surface is prohibitively computationally expensive for optimization over multiple microcell configurations. For this reason, we develop our own simplified model. To approximate the 3D problem using our 2D formulation for each direction (θ,ϕ), we calculate path lengths and average Fresnel coefficients and average them over several hundred azimuth angles ϕ, for satisfactory convergence, so that all model parameters depend only on θ.

The waveguiding structure is assumed to support plane-wave modes with propagation directions θ, obtained using a random number generator. Each propagating mode is considered to be statistically independent. Besides its propagation direction, each mode is also characterized by its spectral irradiance F_θ. As a mode travels inside an absorbing material, its spectral irradiance changes in accordance with Beer-Lambert Law, or,

$$F_\theta(\lambda) = \langle F_{\theta 0}(\lambda,\phi)\exp(-\alpha(\lambda)d(\theta,\phi))\rangle_\phi, \quad (6)$$

where $\alpha(\lambda)$ is the absorption coefficient, d is the distance travelled, $F_{\theta 0}(\lambda)$ is the initial spectral irradiance, and θ is the direction of propagation of an angular mode.

At all interfaces other than the diffuse reflector surface, the spectral irradiance of a mode is transformed in accordance with the Fresnel law for random polarization, given by

$$R_{\mathrm{rp}}(\theta,\phi)=\frac{1}{2}(R_{\mathrm{TM}}(\theta,\phi)+R_{\mathrm{TE}}(\theta,\phi)), \tag{7a}$$

$$T_{\mathrm{rp}}(\theta,\phi)=\frac{1}{2}(T_{\mathrm{TM}}(\theta,\phi)+T_{\mathrm{TE}}(\theta,\phi)), \tag{7b}$$

and the propagation direction of a mode changes at an interface in accordance with Snell's law.

At the reflector surface, the spectral irradiance of a mode is coupled to all other angular modes according to the relation

$$F_{\theta}(\lambda)=F_{\theta'}(\lambda)\langle R(\lambda,\theta,\theta',\phi)\rangle_{\phi}, \tag{8}$$

where θ is a reflected mode, θ' is the incident mode, and R_0 is reflectivity of the reflector. For a Lambertian diffuse reflector, the scattered mode intensity is independent of θ' as indicated by the last term in (8).

Multiple generations of photons are taken into account, and for each photon generation, the photon flux absorbed by the kth microcell is given by

$$\Phi_{\mathrm{abs},k}=\frac{1}{hc}\int_0^{\lambda_g}\sum_{i=1}^{M}\sum_{n=1}^{N}\langle F_{0,i}(\lambda,\theta_n,\phi)\times(1-\exp(-\alpha(\lambda)d(\theta_n,\phi)))\rangle_{\phi}\lambda\mathrm{d}\lambda, \tag{9}$$

where i is the ray generation, n is the angular mode with a random propagation direction θ_n, $\alpha(\lambda)$ is the wavelength-dependent Si absorption coefficient, d is the distance travelled by a ray inside the microcell semiconductor material, h is Planck's constant, and c is the speed of light. The multiple scattering process continues until the absorbed power P_{abs} converges, which determines how may ray generations, M, and how many independent angular modes, N, one needs to consider.

Along an optical ray path, absorption and luminescence inside a luminescent dye-doped film are described by the coupled integro-differential Eqs. (10a) and (10b), and the finite-difference approximation to these equations used in the model is given by Eq. (10c)

$$\frac{dF_l(x,\lambda)}{dr_i}=-\alpha(\lambda)F_l(r_i,\lambda)+\eta_q(\lambda)\varepsilon_0(\lambda)\times\int_0^{\lambda}\alpha(\lambda')(F_l(r_j,\lambda')+F_{nl}(r_j,\lambda'))\lambda'\mathrm{d}\lambda'/\int_0^{\lambda}\lambda'\mathrm{d}\lambda', \tag{10a}$$

$$\frac{dF_{nl}(r_i,\lambda)}{dr_i}=-\alpha(\lambda)F_{nl}(r_i,\lambda), \tag{10b}$$

$$F_l(\lambda,\theta,\phi,L(\theta))=\eta_q\varepsilon_0(\lambda)\exp(-\alpha(\lambda)\Delta L(\theta,\phi))\times\frac{\int(1-\exp(-\alpha(\lambda')\Delta L(\theta)))(F_l(\lambda',\theta,\phi,\Delta L(\theta))+F_{nl}(\lambda',\theta,\phi,\Delta L(\theta)))\lambda'\mathrm{d}\lambda'}{\int\lambda'\mathrm{d}\lambda'},\ \lambda'<\lambda, \tag{10c}$$

where $\Delta L(\theta,\phi)$ is a finite-difference step along a ray, $\varepsilon_0(\lambda)=\frac{\varepsilon(\lambda)}{\int\varepsilon(\lambda')\mathrm{d}\lambda'}$ is the normalized emission spectrum, $\varepsilon(\lambda)$ has the maximum of $1/N_{\mathrm{ray}}$, where N_{ray} is the number of rays per 4π steradian solid angle, λ' is the absorbed wavelength, $\eta_q(\lambda)$ is the quantum yield of the dye, $\alpha(\lambda')$ is the absorption coefficient, and $F_{nl}(\lambda,\theta,\phi,L(\theta,\phi))$ and $F_l(\lambda,\theta,\phi,L(\theta,\phi))$ are the nonluminescent and luminescent portions of the spectral irradiances, respectively. Equation (10c) considers the self-absorption of the luminescent medium and is applied to multiple rays, so that the isotropic emission of the dye is also taken into account. To reduce the discretization errors in this finite-difference approach, each ray is subdivided into small steps, chosen separately for each wavelength, so that $\alpha(\lambda)\Delta L\ll 1$. In this analysis, the dye concentration range has been selected so that there is no emission self-quenching and that the internal quantum efficiency of the dye is constant.

3. Results and Discussion

The performance of the system depends sensitively on the absorptivity and reflectivity of the Si, and the absorption and emission spectra of the fluorescent dyes. Figure 2(a) shows the normal reflectivity of the Si embedded in an NOA 61 polymer layer and the Si absorption coefficient, both as functions of the light wavelength [14]. Figure 2(b) shows the absorption and emission spectra of DCM fluorescent dye. In the experimental work accompanying this study, the complex refractive index of the NOA polymer and the absorption/emission spectra of the dyes are measured using a spectrophotometer [1].

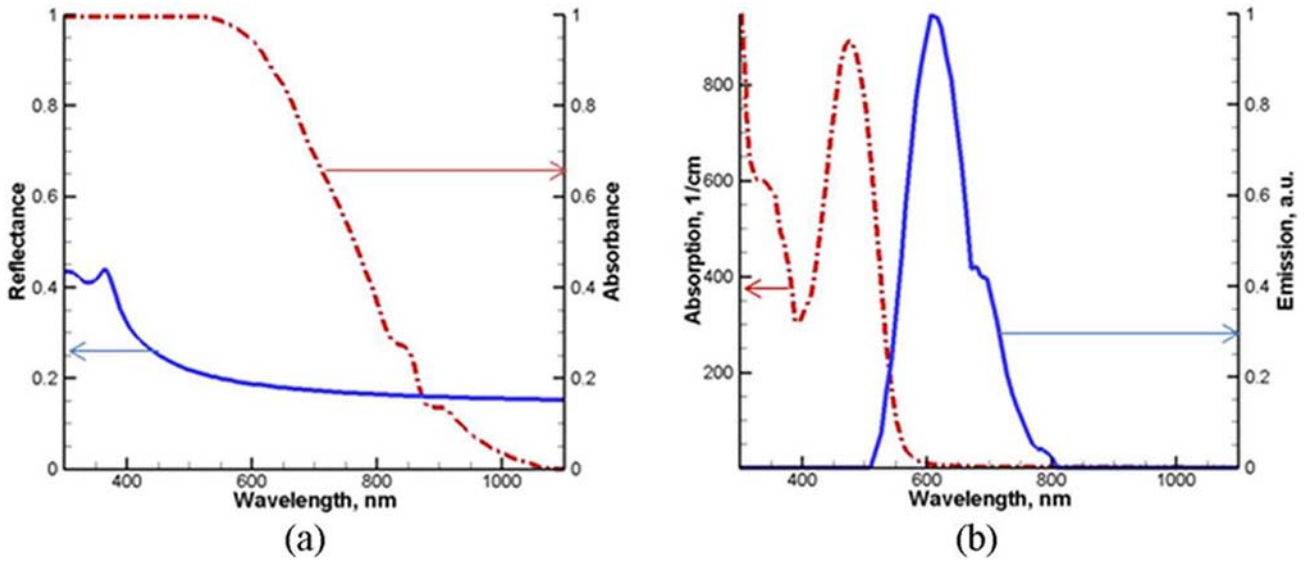

Fig. 2. (Color online) Optical properties. (a) Si normal reflectance in NOA and 15 μm Si slab normalized absorbance, Si properties from [13], (b) absorption and emission spectra for DCM.

It can be seen from Fig. 2(a) that the surface reflectivity at a planar Si-polymer interface is high at short light wavelengths, contributing to substantial absorbed photon flux losses. The DCM dye absorbs photons at those wavelengths and emits photons in the longer wavelength range where the Si surface reflectivity is lower. Therefore, the indirect gain is affected by both the ratios of surface reflectances of Si at the dye absorption and emission wavelengths and the associated conversion (thermalization) losses. At the peak emission wavelength of the dye, Si absorptivity is relatively high and is not expected to reduce the absorbed photon flux for a typical microcell thickness of 15 μm. In our model, we consider Si absorption between 300 and 1100 nm. In our models, we also consider the typical dye concentrations that correspond to the absorbance $A = 0.5$ across a 30 μm NOA:DCM film at the DCM absorption peak wavelength of 476 nm. The geometry used in the model is a microcell array consisting of 21 silicon microcells with the variable parameters W, t, s, and a. The thickness of the waveguiding layer is constant, $a_{\mathrm{NOA}} = 30\,\mu$m. A part of microcell array cross section is shown schematically in Fig. 1. The aspect ratio of the actual Si microcells in the x-y plane is about 30 [1]. Because of such a high aspect ratio, the actual 3-D design is represented as 2D geometry, infinitely extended along the y axis, without a significant loss of accuracy, provided that the transport of photons is averaged over all azimuth (x-y plane) angles. Figures 3(a) and 3(b) show our simulation results for the solar concentrator indirect gains. The calculations are experimentally validated in [15], and the corresponding experimental results are also presented in Fig. 3(c).

The results shown in Fig. 3 refer to a single microcell in the middle of a 21-cell array. The absorbed photon flux is found to be ~10%–30% higher for the first three microcells from the edge due to their contact with luminescent dye-filled wide gaps and the resulting increase in the effective area from which solar photons are harvested, but a microcell in the center of the array absorbs almost the same number of photons as the same microcell in an infinite array. Figure 3(a) shows the indirect gain provided by the nonluminescent solar concentrator as a function of the Si area fill factor, $W/(W+s)$, and the microcell width W, for the glass substrate layer

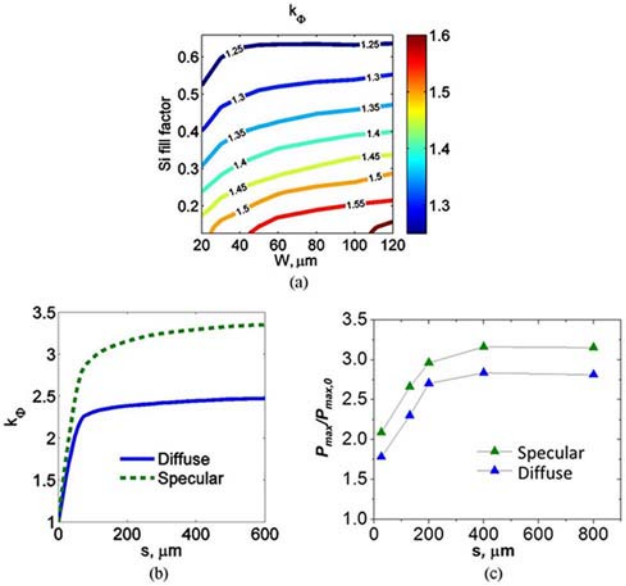

Fig. 3. (Color online) Indirect gain (a) as a function of the microcell fill factor and microcell width, predicted for with a nonluminescent concentrator, $t = 15\,\mu$m, $a = 1000\,\mu$m (glass substrate), (b) predicted for luminescent concentrators with DCM dye (specular, $R_0 = 0.98$, and diffuse reflectors, $R_0 = 0.93$), $W = 50\,\mu$m, $a = 1000\,\mu$m (glass substrate), (c) measured for luminescent concentrators with DCM dye (specular, $R_0 = 0.98$, and diffuse reflectors, $R_0 = 0.93$), $W = 50\,\mu$m, $a = 1000\,\mu$m (glass substrate), as in [15].

($n_r = 1.45$) thickness $a = 1000\,\mu$m and microcell thickness $t = 15\,\mu$m.

As seen from Fig. 3(a), the indirect gain increases as the microcell fill factor decreases (or as the separation s between the microcells increases). The curve asymptotically approaches a saturation level. For practical purposes, we consider the saturation point to be 0.95 of the plateau value. The increase in k_Φ, with decreasing cell width W and a constant layer thickness a, is a geometric effect related to the finite width of an array and is discussed later in the text. Figure 3(b) shows the calculated indirect gain for the nonluminescent waveguiding concentrator as a function of the Si microcell separation for $W = 50\,\mu$m, $a = 1000\,\mu$m (glass substrate), R_0 is assumed to be 0.93. Our simulations suggest that by dispersing the DCM dye in the polymer film embedding the microcells, the saturation value of indirect gain k_Φ can be increased from 1.9 to 2.45 for the diffuse reflector, and up to 3.3 for the specular reflector. The increase in the number of absorbed photons with the increasing gap between the PV microcells is due to indirect illumination collected from a larger area. This is a well-known result for solar concentrators that guide light due to TIR [9,10]. The spacing of about 100–200 μm between the microcells, at which the saturation occurs, is short compared to the photon flux extinction length due to the photon self-absorption in the dye-doped layer which is on the order of tens of thousands of micrometers. The experimental results presented in Fig. 3(c) show reasonable agreement with our simulations. The differences in magnitude are mainly due to the additional areas exposed to incident light in our experiments.

The collection efficiency from our simulations, defined as the indirect solar irradiance absorbed in the PV microcells, normalized by the indirect input irradiance into the collector, can be substantially higher compared to the values reported in previous work on luminescent concentrators [16,17]. Based on our findings, the higher efficiencies of the waveguiding concentrators with microcells along the top surface are due to the differences in the concentrator geometries.

To quantify how the glass substrate thickness affects the indirect gain, the latter is calculated at fixed cell widths of $W = 50\,\mu$m and the microcell fill factor of 0.11 and varying thicknesses, a. The corresponding dependences are shown in Fig. 4(a).

Figure 4(b) presents the indirect gain as a function of the cell thickness for a Si microcell array embedded in a nonluminescent polymer layer and backed by a diffuse BSR, normalized by the absorbed photon flux in a very thick Si microcell (nearly full absorption). Geometric parameters used in this simulation are $W = 50\,\mu$m, $s = 345\,\mu$m, and $a/W = 20$.

Simulations with the variable substrate thickness [Fig. 4(a)] show substantial reductions in the absorbed photon flux when the reflector is far from the microcells. This limit can be attributed to the finite extent of the microcell array, causing a larger

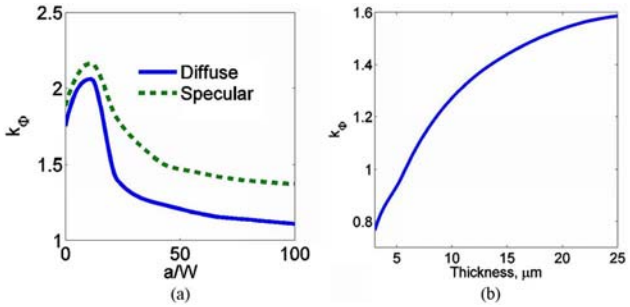

Fig. 4. (Color online) (a) Dependence of the indirect gain on the distance between the microcells and the backside reflector for the nonluminescent and luminescent solar concentrators ($W = 50\,\mu$m, microcell fill factor is 0.11). The optimal value of an a/W is approximately 10. (b) Effect of microcell thickness on the light absorption relative to a very thick Si slab, in the presence of the diffuse BSR, with $a/W = 20$, $W = 50\,\mu$m, and constant microcell fill factor = 0.126. In both cases, glass substrates are assumed.

fraction of photons to escape from the microcell array laterally at larger a. A small reduction in the indirect gain when the reflector is close to the microcells is seen only for relatively large gaps between the cells ($s/W > 4$).

In case the refractive indices of the embedding polymer and the substrate are substantially different, for example if their refractive index ratio is 1.8:1.45 instead of ~1.6:1.45, as for the (NOA 61)-glass system, the indirect gain is reduced by about 4%. This result means that for the polymer refractive index of 1.8, an improvement in the waveguiding due to TIR is smaller than the additional photon flux losses due to the higher reflectivity at the air-polymer interface and also due to the changes in the angular distribution of the rays in the substrate, causing higher percentages of the photons to escape from the structure laterally. TIR-based confinement of light, thus, has limitations that cannot be simply overcome by simply increasing the refractive index of the waveguiding layer.

Another parameter that is important for our design is the thickness of the Si microcells. The absorption coefficient of silicon [Fig. 2(a)] is low for wavelengths longer than 700 nm, and the sufficient microcell thickness is critical at longer wavelengths, unless light-trapping is utilized. The calculated dependences of the indirect gain on the microcell fill factor and the microcell thickness are presented in Fig. 5. Since the dye concentration and the reflector properties are expected to significantly affect the indirect gain of the concentrator, these results are only shown for a nonluminescent case, assuming an ideal diffuse reflector with $R_0 = 1$, $W = 50\,\mu$m, glass substrate, and $a = 1000\,\mu$m.

As our results show in Fig. 5, the value of the indirect gain increases with increasing microcell thickness and with decreasing microcell fill factor. The thicknesses of Si microcells affect the indirect gain due to both the light-trapping and the increase in indirectly illuminated surface areas of the cells. Both mechanisms contribute to the higher device

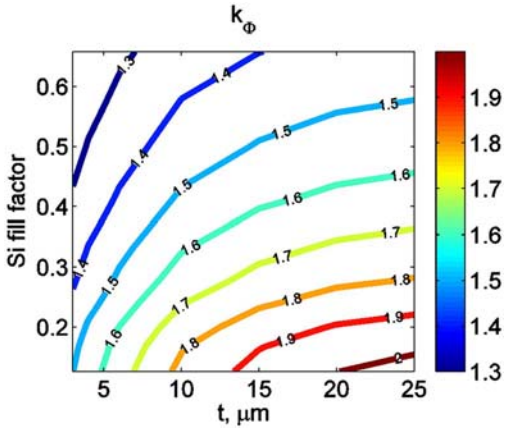

Fig. 5. (Color online) Indirect gain of a Si microcell array with a nonluminescent concentrator as a function of the microcell fill factor and microcell thickness. $W = 50\,\mu$m, $a = 1000\,\mu$m, glass substrate, ideal Lambertian reflector.

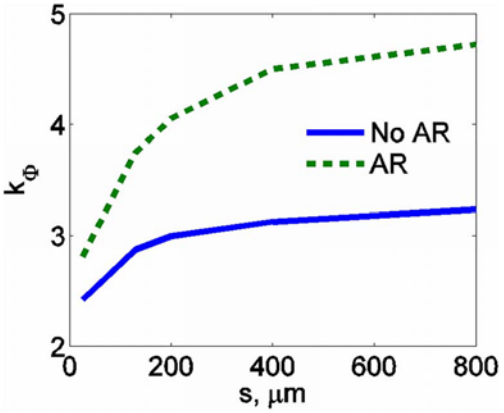

Fig. 7. (Color online) Indirect gain of a microcell array with and without ideal AR surfaces as a function of separation between microcells, $W = 50\,\mu$m, $a = 1000\,\mu$m, glass substrate, luminescent solar concentrator, specular reflector, and $R_0 = 0.98$.

efficiency. The Si microcell thickness, taking into account our results shown in Fig. 4(b), should be chosen to be approximately $8\,\mu$m or more, to avoid severe reductions in the absorbed photon flux, unless special light-trapping schemes are applied.

Figure 6 shows dependences of the indirect gain of the luminescent and nonluminescent solar collectors with the specular reflector ($R_0 = 0.98$) on the radius of NOA substrate curvature in the x-z plane normalized by the array width. In this simulation, $W = 50\,\mu$m, $s = 100\,\mu$m, the number of silicon microcells is 21, and the NOA substrate layer is $30\,\mu$m thick. The total width of the collector is $10{,}000\,\mu$m.

For the deformed solar concentrators with specular reflectors, the indirect gain decreases with the diminishing radius of curvature, when calculated in reference to a flat collector, due to the reduction in the projected area. When these calculated results

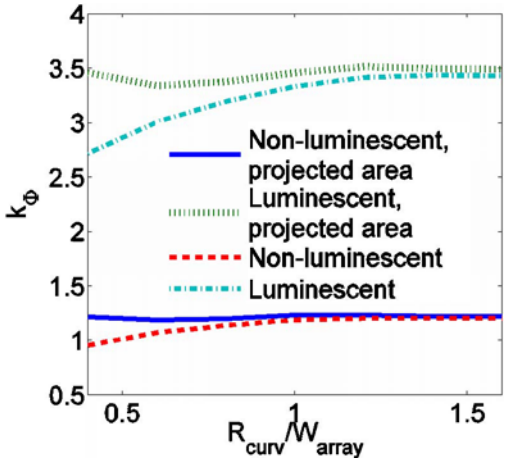

Fig. 6. (Color online) Indirect gain of a deformed Si microcell array, $W = 50\,\mu$m, $s = 100\,\mu$m, $a = 30\,\mu$m with luminescent and nonluminescent concentrators, specular reflector, $R = 0.98$, as a function of the bending radius normalized to the width of substrate. Curves labeled "projected area" show indirect gains calculated with the normalization to a flat system with the same projected area.

are renormalized by the projected area, the dependences of the collector indirect gain on the radius of curvature are almost flat.

Reflectivities of top and side microcell surfaces can be reduced by applying antireflection coatings. In the next case we assume that all the surfaces are roughened, so that their reflectivities are neglected. We calculate the indirect gain as a function of the spacing between microcells for the ideal AR case, and the corresponding results, in comparison with the specular reflector luminescent case [Fig. 3(b)], are presented in Fig. 7. All simulation parameters are the same in both cases, except for the Si surface reflectivities.

Comparing the results in Fig. 7 for the microcells with and without the AR coatings, one can see that by reducing the surface reflectances, the absorbed photon flux and the cell photocurrent can be boosted by a factor of up to 1.46 (for an ideal ARC).

To study how the spectral properties of the luminophore would affect the performance of our solar concentrator, we considered a generic fluorophore characterized by the absorption spectrum of the DCM dye (since a functional form of its absorption spectrum is not practical for the model), and whose emission spectrum is modeled as a Lorentzian function with just two variable parameters: the central wavelength, varied from 570 to 650 nm, and the half-maximum width, varied from 90 to 150 nm. The highest absorbed photon flux is predicted for the following parameters: emission peak wavelength, 630 nm; emission peak width, 150 nm; Stokes shift between the absorption and emission central wavelengths, 154 nm. Thus, the current DCM dye (emission peak wavelength 652 nm, Stokes shift 176 nm, half-maximum width 140 nm) is reasonably close to the optimum case, and the expected deviation from the absorbed photon flux for that ideal dye is less than 2%. Given the absorption spectrum of the DCM dye, the concentrator indirect gain is found to be relatively insensitive to the peak emission wavelength for the Stokes shifts larger than 100 nm.

4. Conclusions

Based on our modeling results, we conclude that waveguiding solar concentrators with the microcells embedded into the top surface of the waveguiding layer can substantially improve the absorption of solar photons in flexible ultrathin solar microcell arrays. Our calculations are validated by the accompanying experiments for a simple nonluminescent waveguiding concentrator as well as for a luminescent concentrator [15].

As the separation between the PV microcells increases, the absorbed photon flux increases, until it reaches saturation. The specific geometry of our flexible PV microcell arrays allows more efficient utilization of the incident solar energy compared to the solar concentrators with side-mounted cells because the spacings between microcells can be tailored to match the saturation of the absorbed photon flux of the concentrator. Thereby, high photon collection efficiencies can be achieved. Other geometric parameters also play an important role—with the increasing microcell thickness, the indirect gain is enhanced due to the longer photon path in Si, as well as due to the higher indirectly illuminated microcell surface area. The thickness of Si microcells, their mechanical properties notwithstanding, should be chosen sufficiently large to absorb most of the long-wavelength solar spectrum, up to the Si bandedge of 1130 nm. The reflector has less effect on the device's external quantum efficiency at the wavelengths where the Si absorption is low, and additional light-trapping schemes such as nanoscale diffractive antireflection surfaces may be explored. Also, the width of the microcell in relation to the thickness of the substrate layer (assuming a good refractive index match between the polymer and the substrate layers) needs to be chosen sufficiently large, so that $a/W \leq 10$.

The extinction length of the waveguided light due to self-absorption in our dye-doped concentrator design is considerably longer than the typical spacings between microcells, thus, this concentrator, unlike many of the previous implementations, is not limited by self-absorption losses. The effects of the dye self-absorption on the indirect gain are minor. From our model, we find that the DCM dye has emission properties that are close to optimal, for the case of silicon microcells.

Antireflection coatings can be applied on all microcell surfaces, thereby increasing the numbers of photons admitted and absorbed due to both direct and indirect illumination. For Si microcells, the indirect gain can be increased by about 46% due to an ARC compared to the "no ARC" case.

The indirect photon flux using our nontracking solar concentrators is also affected by the scattering properties of the reflector as well as by the spectral matching between the luminescent dye emission and the low-reflectivity wavelength range of the semiconductor material embedded in a polymer layer. Specifically, in a nonluminescent waveguiding concentrator, only a diffuse reflector can substantially increase the indirect photon flux absorbed in Si. A luminescent concentrator, on the other hand, can have a diffuse or specular reflector, or a dielectric-dielectric interface with the refractive indices of the guiding layer and substrate chosen so that photons can be guided by total internal reflection, since the luminescent medium randomizes the photon directions.

According to our model, a luminophore inside the waveguiding polymer layer should significantly increase the saturation value of the indirect gain as a function of the intercell distance, compared to a nonluminescent concentrator with the same geometry.

When a flexible microcell array backed with a specular reflector is bent, the photon flux absorbed by all microcells shows no reduction in the indirect gain compared to a flat solar concentrator with the projected same area. This is due to a higher portion of the incident flux redirected towards μ-cells in the curved dielectric waveguide and also due to the isotropic emission of the luminescent dye which is invariant to the incidence direction.

This work is supported by the Department of Energy, through grant no. DE-FG02-07ER46471 at the Frederick Seitz Materials Research Laboratory at the University of Illinois.

References

1. J. Yoon, A. J. Baca, S. Park, P. Elvikis, J. B. Geddes, L. Li, R. H. Kim, J. Xiao, S. Wang, T.-H. Kim, M. J. Motala, B. Y. Ahn, E. B. Duoss, J. A. Lewis, R. G. Nuzzo, P. M. Ferreira, Y. Huang, A. Rockett, and J. A. Rogers, "Ultrathin silicon solar microcells for semitransparent, mechanically flexible and microconcentrator module designs," Nat. Mater. **7**, 907–915 (2008).
2. J. S. Batchelder, "Luminescent solar concentrators. 1: Theory of operation and techniques for performance evaluation," Appl. Opt. **18**, 3090–3110 (1979).
3. A. Goetzberger and W. Greubel, "Solar energy conversion with fluorescent collectors," Appl. Phys. **14**, 123–139 (1977).
4. V. Wittwer, W. Stahl, and A. Goetzberger, "Fluorescent planar concentrators," Sol. Energy Mater. **11**, 187–197 (1984).
5. A. A. Earp, G. B. Smith, P. D. Swift, and J. Franklin, "Maximising the light output of a luminescent solar concentrator," Solar Energy **76**, 655–667 (2004).
6. G. Smestad and P. Hamill, "Concentration of solar radiation by white backed photovoltaic panels," Appl. Opt. **23**, 4394–4402 (1984).
7. G. Lifante, F. Cusso, F. Meseguer, and F. Jaque, "Solar concentrators using total internal reflection," Appl. Opt. **22**, 3966–3970 (1983).
8. D. Marcuse, *Theory of Dielectric Optical Waveguides* (Academic, 1991).
9. T. Bierhoff, E. Griese, and G. Mrozynski, "An efficient Monte Carlo based ray tracing technique for the characterization of highly multimode dielectric waveguides with rough surfaces," in *Proceedings of the 30th European Microwave Conference, 2000*, Paris, France, Vol. 1, (Horizon House, 2000), pp. 379–382.
10. T. Bierhoff, A. Wallrabenstein, A. Himmler, E. Griese, and G. Mrozynski, "Ray tracing technique and its verification for the analysis of highly multimode optical waveguides with rough surfaces," IEEE Trans. Magn. **37**, 3307–3310 (2001).
11. Norland Optical Adhesive 61, https://www.norlandprod.com/adhesives/NOA%2061.html.

12. ASTM G173-03, http://rredc.nrel.gov/solar/spectra/am1.5/.
13. N. P. Buslenko, D. I. Golenko, Y. A. Shreider, I. M. Sobol, and V. G. Sragovich, *The Monte Carlo Method. The Method of Statistical Trials*, Y. A. Shreider, ed. (Pergamon, 1966).
14. Virginia Semiconductor, Inc., Optical properties of silicon (2004).
15. J. Yoon, L. Li, A. V. Semichaevsky, H. T. Johnson, R. Nuzzo, and J. A. Rogers, "Flexible luminescent concentrator photovoltaics based on sparse, embedded arrays of microscale silicon solar cells," Nat. Comm. (in press).
16. M. J. Currie, J. K. Mapel, T. D. Heidel, S. Goffri, and M. A. Baldo, "High-efficiency organic solar concentrators for photovoltaics," Science **321**, 226–228 (2008).
17. L. R. Wilson, B. C. Rowan, N. Robertson, O. Moudam, A. C. Jones, and B. S. Richards, "Characterization and reduction of reabsorption losses in luminescent solar concentrators," Appl. Opt. **49**, 1651–1661 (2010).